

Collectivity at $N = 50$: ^{82}Ge and ^{84}Se

A. Gade,^{1,2} T. Baugher,^{1,2} D. Bazin,¹ B. A. Brown,^{1,2} C. M. Campbell,¹ T. Glasmacher,^{1,2} G. F. Grinyer,¹ M. Honma,³ S. McDaniel,^{1,2} R. Meharchand,^{1,2} T. Otsuka,^{4,5} A. Ratkiewicz,^{1,2} J. A. Tostevin,⁶ K. A. Walsh,^{1,2} and D. Weisshaar¹

¹*National Superconducting Cyclotron Laboratory, Michigan State University, East Lansing, Michigan 48824*

²*Department of Physics and Astronomy, Michigan State University, East Lansing, Michigan 48824*

³*Center for Mathematical Sciences, University of Aizu, Tsuruga,*

Ikki-machi, Aizu-Wakamatsu, Fukushima 965-8580, Japan

⁴*Department of Physics and Center for Nuclear Study,*

University of Tokyo, Hongo, Tokyo 113-0033, Japan

⁵*RIKEN, Hirosawa, Wako-shi, Saitama 351-0198, Japan*

⁶*Department of Physics, Faculty of Engineering and Physical Sciences,*

University of Surrey, Guildford, Surrey GU2 7XH, United Kingdom

(Dated: November 15, 2021)

The neutron-rich $N = 50$ isotones ^{82}Ge and ^{84}Se were investigated using intermediate-energy Coulomb excitation on a ^{197}Au target and inelastic scattering on ^9Be . As typical for intermediate-energy Coulomb excitation with projectile energies exceeding 70 MeV/nucleon, only the first 2^+ states were excited in ^{82}Ge and ^{84}Se . However, in the inelastic scattering on a ^9Be target, a strong population of the first 4^+ state was observed for ^{84}Se , while there is no indication of a similarly strong excitation of the corresponding state in the neighboring even-even isotope ^{82}Ge . The results are discussed in the framework of systematics and shell-model calculations using three different effective interactions.

I. INTRODUCTION

The selenium and germanium isotopic chains exhibit a complex nuclear structure and have long been a rich testing ground for nuclear structure models. Their properties are driven by shape coexistence and rapid shape changes all the way from the $N = Z$ line into the $A \approx 70$ mass region [1–13]. On the other side of the nuclear chart, the most neutron-rich selenium and germanium isotopes accessible for experiments are around the magic neutron number $N = 50$. Considerable experimental and theoretical efforts have recently been focused in this region on the investigation of the shell structure approaching the doubly-magic nucleus ^{78}Ni , see for example [14–18]. The description of nuclei in this region poses a challenge for shell-model calculations since the full pf shell and the neutron $g_{9/2}$ intruder orbital would be needed with the corresponding effective interaction. Presently, smaller configuration spaces have to be used, typically starting from a ^{56}Ni core and including the $p_{3/2}$, $f_{5/2}$, $p_{1/2}$ and $g_{9/2}$ orbitals [19, 20]. Experimental information is important to guide the emerging shell-model effective interactions in this region.

In the present paper we report the experimental results of the intermediate-energy projectile Coulomb excitation and inelastic scattering on a ^9Be target for the $N = 50$ isotones ^{82}Ge and ^{84}Se . While Coulomb excitation with fast projectile beams allows for the sensitive study of the $B(E2; 0_{gs}^+ \rightarrow 2_1^+) \equiv B(E2 \uparrow)$ excitation strength in even-even nuclei – a measure of the low-lying quadrupole collectivity – ^9Be -induced inelastic scattering provides access to collective structures beyond the first 2^+ state. Measured $B(E2 \uparrow)$ electric quadrupole excitation strengths along line of $N = 50$ isotones are compared

to large-scale shell-model calculations with three different effective interactions. The evolution of collectivity along the Se and Ge chains is further confronted with mean-field calculations. The population of higher-lying states in the ^9Be -induced inelastic scattering of ^{84}Se is discussed in comparison to inelastic proton and α scattering on stable selenium isotopes.

II. EXPERIMENT

The measurements were performed at the National Superconducting Cyclotron Laboratory (NSCL) on the campus of Michigan State University. The neutron-rich projectile beams containing ^{82}Ge and ^{84}Se were produced in-flight by fragmentation of a 140 MeV/u ^{86}Kr primary beam provided by the Coupled-Cyclotron Facility at NSCL. ^9Be foils with thicknesses of 432 mg/cm² and 329 mg/cm², respectively, served as production targets for the two different secondary beams. The fragments of interest were selected with the A1900 fragment separator [21]; an achromatic 210 mg/cm² aluminum wedge degrader located at the mid-acceptance position of the fragment separator was used. The total momentum acceptance was restricted to 2% for ^{82}Ge and 1% for ^{84}Se . The setting optimized on ^{84}Se resulted in a pure ($> 99.5\%$) secondary beam. The purity of the cocktail beam containing ^{82}Ge was 32%.

Gold and beryllium targets used to induce projectile Coulomb excitation and inelastic scattering, respectively, were located at the target position of the S800 spectrograph [22]. The identification of the scattered projectiles and the trajectory reconstruction used to derive the scattering angles on an event-by-event basis utilized the de-

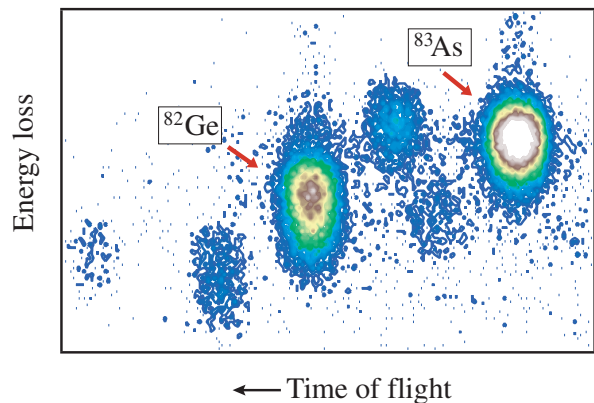


FIG. 1: (Color online) Particle identification for the cocktail beam optimized on ^{82}Ge after interaction with the gold target. Plotted is the energy loss measured with the S800 ionization chamber versus the time of flight measured between the plastic trigger scintillator at the back of the S800 focal plane and a timing scintillator at the spectrograph’s object position.

tection systems of the spectrograph’s focal plane, consisting of an ionization chamber, two xy-position-sensitive cathode-readout drift chambers and a plastic timing scintillator [23]. An example of the identification of the scattered projectiles emerging from the gold target is shown in Fig. 1 for the setting optimized on ^{82}Ge , where the energy loss measured with the S800 ionization chamber versus the ion’s time of flight measured between two plastic scintillators is displayed. ^{82}Ge can be clearly separated from the other constituents of the cocktail beam that contained ^{83}As as the largest contaminant.

The reaction target located in front of the S800 spectrograph was surrounded by the high-resolution γ -ray detection system SeGA, an array of 32-fold segmented high-purity germanium detectors [24]. The segmentation of the detectors allowed for an event-by-event Doppler reconstruction. The angle of the γ -ray emission was deduced from the position of the segment that registered the highest energy deposition. The detectors were arranged in two rings (90° and 37° central angles with respect to the beam axis). The 37° ring was equipped with seven detectors, while ten and nine detectors were located at 90° for the Coulomb excitation and ^9Be -induced inelastic scattering measurements, respectively. The energy-dependent photopeak efficiency of the setups was determined with standard ^{152}Eu and ^{226}Ra calibration sources.

III. RESULTS AND DISCUSSION

A. Intermediate-energy Coulomb excitation

Coulomb excitation is a widely used experimental technique to assess the low-lying quadrupole collectivity in nuclei. In projectile Coulomb excitation, exotic nuclei,

produced as beams of ions, are scattered off stable high- Z targets and are detected in coincidence with the de-excitation γ rays that tag and quantify the inelastic process [25–27]. While beam energies below the Coulomb barrier prevent nuclear contributions to the excitation process, very peripheral collisions must be chosen in the regime of intermediate-energy Coulomb scattering to exclude nuclear contributions. This can be realized by restricting the data analysis to scattering events at very forward angles, corresponding to large minimum impact parameters, b_{min} , in the collisions of projectile and target nuclei [25]. Impact parameters exceeding $1.2(A_p^{1/3} + A_t^{1/3}) + 2$ fm (“touching sphere + 2 fm”) have been proven sufficient to ensure the dominance of the electromagnetic interaction [28–30].

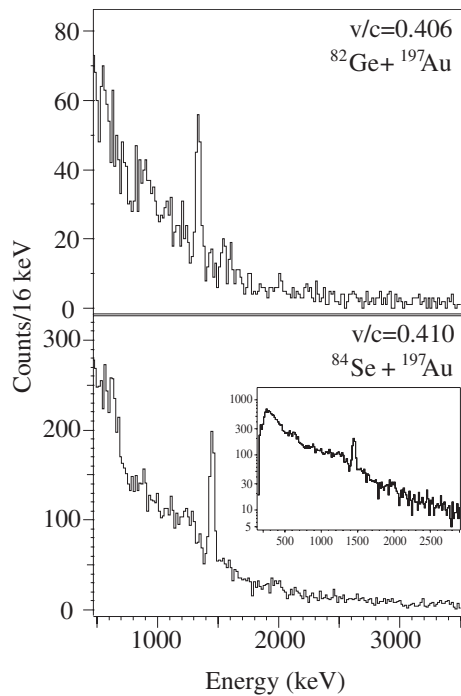


FIG. 2: Projectile Coulomb excitation of ^{82}Ge (upper panel) and ^{84}Se (lower panel). The γ -ray energies are event-by-event Doppler reconstructed into the rest frame of the projectile using the angle information obtained from the segmentation of the SeGA detectors. Only one γ -ray transition, the de-excitation of the 2_1^+ state, was observed in each nucleus. The inset shows a wider range of the ^{84}Se γ -ray spectrum on a logarithmic scale; no other transitions were observed.

In the present work, gold targets of thicknesses 256 mg/cm^2 and 184 mg/cm^2 for ^{82}Ge and ^{84}Se , respectively, were used to induce the Coulomb excitation. The mid-target energies of the ^{82}Ge and ^{84}Se beams were 89.4 $\text{MeV}/\text{nucleon}$ and 95.4 $\text{MeV}/\text{nucleon}$, respectively, resulting in a minimum impact parameter of $b_{min} = 14.2$ fm for both the $^{82}\text{Ge}+^{197}\text{Au}$ and $^{84}\text{Se}+^{197}\text{Au}$ collisions. Correspondingly, maximum scattering angles in the laboratory system of $\theta_{max} = 2.05^\circ$ and 1.99° were chosen for the analysis of ^{82}Ge and ^{84}Se , respectively.

The target Coulomb excitation of the first excited $7/2^+$ state in ^{197}Au by the electromagnetic field of the projectiles passing through the target was observed. Figures 2 and 3 show the γ -ray spectra detected in coincidence with the different scattered projectiles.

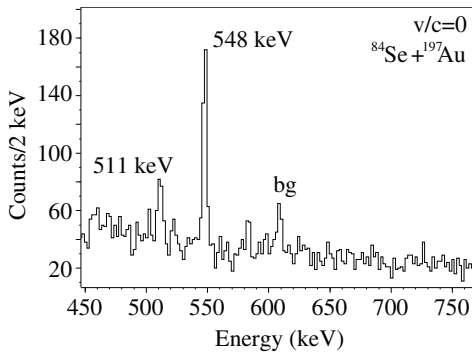


FIG. 3: Coulomb excitation of ^{197}Au induced by the ^{84}Se projectile beam passing through the gold target (laboratory frame, $v/c = 0$). The γ -ray transition corresponds to the de-excitation of the 547.5 keV $7/2^+$ state to the $3/2^+$ ground state.

Angle-integrated Coulomb excitation cross sections $\sigma(\theta \leq \theta_{max})$ were determined from the efficiency-corrected γ -ray intensities of the $2_1^+ \rightarrow 0_{gs}^+$ transitions relative to the number densities of the gold targets and the number of projectiles passing through the targets. The efficiencies were corrected for the Lorentz boost and the γ -ray angular distribution in intermediate-energy Coulomb excitation [31] and absorption in the gold target. The semi-classical Winther-Alder theory [31] was used to derive $B(E2 \uparrow)$ excitation strengths from the angle-integrated cross sections. To test the setup and analysis procedures, the $B(E2; 3/2^+ \rightarrow 7/2^+)$ electromagnetic transition strength in ^{197}Au was determined from the Coulomb excitation of the ^{197}Au target induced by the ^{82}Ge , ^{83}As and ^{84}Se projectiles. Table I summarizes the angle-integrated Coulomb excitation cross sections and extracted $B(E2 \uparrow)$ values. The results for ^{82}Ge and ^{197}Au from this work agree with the literature values [32, 33].

Figure 4 shows the systematics of the reduced electric quadrupole excitation strength $B(E2; 0^+ \rightarrow 2_1^+)$ for the $N = 50$ isotones from zinc to molybdenum. The experimental results are compared to shell-model calculations using the jj4b, jj4pna [14] and the JUN45 [20] effective interactions. Similar to the work on $E2$ transition rates in $N = 50$ isotones by Ji and Wildenthal [34], proton effective charges of $e_p \approx 2$ were used [55]. The need for a rather large proton effective charge, compared to $e_p = 1.5$ typical for calculations in the sd shell, for example, is indicative of missing neutron core excitations across the $N = 50$ shell gap in the $f_{5/2}, p_{3/2}, p_{1/2}, g_{9/2}$ model space. The three effective interactions differ markedly for ^{82}Ge and ^{84}Se while they show very similar trends at $Z = 30$ and for $Z \geq 36$. Calculations with jj4b and jj4pna agree

TABLE I: Experimental results for ^{82}Ge and ^{84}Se . The mean lifetimes, τ , are deduced from the $B(E2 \uparrow)$ strengths. The Coulomb excitation of the gold target by ^{82}Ge , ^{84}Se and ^{83}As projectiles was quantified as a cross check of the experimental setup and analysis procedures. If available, the literature values are given.

	^{82}Ge	Ref. [33]	^{84}Se	
$E(2_1^+)$ (keV)	1348	1348	1454	1454
$\sigma(\theta \leq \theta_{max})$ (mb)	258(36)		199(22)	
$B(E2 \uparrow)$ ($e^2 b^2$)	0.128(22)	0.115(20)	0.105(15)	-
τ (ps)	0.72(12)	0.80(14)	0.60(9)	-
^{197}Au		Ref. [32]		Ref. [32]
$\sigma(\theta \leq \theta_{max})$ (mb)	152(28)		150(16)	
$B(E2 \uparrow)$ ($e^2 b^2$)	0.476(94)	0.449(41)	0.441(64)	0.449(41)
	0.424(76) ^a			

^aFrom the excitation of the ^{197}Au target by ^{83}As in the cocktail beam that contained ^{82}Ge

with each other and the experimental value for ^{82}Ge while all three interactions differ at ^{84}Se , with JUN45 describing the excitation strength best.

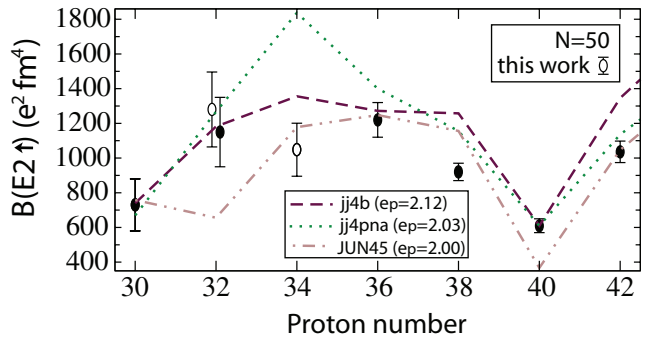


FIG. 4: (Color online) $B(E2; 0^+ \rightarrow 2_1^+)$ systematics of the $N = 50$ isotones. The evolution of quadrupole collectivity along $N = 50$ is compared to shell-model calculations with the jj4b [14] ($e_p = 2.12$), jj4pna [14] ($e_p = 2.03$) and the JUN45 [20] ($e_p = 2.00$) effective interactions. The effective proton charge, e_p , was chosen for each interaction to get closest to the experimental data. The need for fairly high effective charges of $e_p \approx 2$ illustrates the importance of core excitations across the $N = 50$ shell gap which are outside of the employed model space. The experimental data stems from the present work and references [6, 7, 17, 33, 35, 36].

It is apparent from the comparison in Fig. 4 that for the $N = 50$ isotones the calculated $B(E2 \uparrow)$ values of ^{82}Ge and ^{84}Se are particularly sensitive to details of the shell-model effective interaction. The two valence proton orbitals being filled between $Z = 28$ and $Z = 38$ are $f_{5/2}$ and $p_{3/2}$. The sensitivity arises from the details on how these orbitals are occupied. Their filling is largely determined by their effective single-particle energy (ESPE) gap and how it changes between ^{78}Ni and ^{88}Sr . The ESPE were calculated for proton particle states relative

to a ^{78}Ni core and for proton hole states relative to the proton configuration $(f_{5/2})^6(p_{3/2})^4$ (the ^{88}Sr core). The size of the gap, $\epsilon(p_{3/2}) - \epsilon(f_{5/2})$, for the three Hamiltonians is given in Table II along with the ground-state occupancy of the $f_{5/2}$ orbit, $n(f_{5/2})$, in ^{82}Ge and ^{84}Se , respectively. In all three cases, the $f_{5/2}$ orbital ESPE lies below that of the $p_{3/2}$.

TABLE II: Effective single-particle energy (ESPE) gap between $f_{5/2}$ and $p_{3/2}$ and the ground state occupancies for ^{84}Se and ^{82}Ge for the jj4pna, jj4b and JUN45 Hamiltonians.

	$\epsilon(p_{3/2}) - \epsilon(f_{5/2})$ (MeV)		$n(f_{5/2})$	
	^{78}Ni	^{88}Sr	$^{84}\text{Se}_{gs}$	$^{82}\text{Ge}_{gs}$
jj4pna	1.50	0.47	3.81	3.17
jj4b	0.39	0.72	4.00	2.84
JUN45	0.97	1.11	4.40	3.16

In the extreme case of a large gap, the ^{84}Se ground state has an $(f_{5/2})^6$ closed-shell configuration with an occupancy of $n(f_{5/2}) = 6$. For ^{84}Se , the $f_{5/2}$ occupancies are correlated with the ESPE gap in ^{88}Sr . The most highly mixed configuration is obtained with jj4pna and this is associated with a low energy for the excited 2_1^+ (1.18 MeV) together with a $B(E2 \uparrow)$ strength, which is almost twice as large as experiment (see Fig. 4). This is an indication that the $p_{3/2} - f_{5/2}$ ESPE gap for this interaction is too small at $Z = 34$.

The ground state occupancy for ^{82}Ge on the other hand is correlated with the ESPE gap for ^{78}Ni . The JUN45 Hamiltonian gives a $B(E2 \uparrow)$ value which is almost a factor of two smaller than experiment (see Fig. 4). However, for JUN45 there is considerable $E2$ strength to the second 2^+ state at 2.18 MeV (50% of the strength to the 1.50 MeV state). This fragmentation may be related to parts of the Hamiltonian that go beyond the monopole terms that determine the ESPEs.

In Fig. 5, the $B(E2 \uparrow)$ values in the chains of selenium ($A = 68 - 84$) and germanium ($A = 64 - 82$) isotopes are compared to (beyond) mean-field calculations using the constrained Hartree-Fock Bogoliubov (HFB) with mapping on the 5-dimensional collective Hamiltonian [37] approach that uses the D1S Gogny force, abbreviated here by CHFB-5DCH, (upper panel) and to results from HFB calculations using the HFB-17 parameterization [38] (lower panel). For the comparison to HFB-17, the quadrupole deformation parameters β_2 were translated into $B(E2 \uparrow)$ values via $\beta_2 = \frac{4\pi}{3ZR^2} \sqrt{B(E2 \uparrow)}/e^2$, where the sharp-surface radius R was deduced consistently from $R^2 = 5\langle r_c^2 \rangle / 3 - (0.88 \text{ fm})^2$ with $\langle r_c^2 \rangle^{1/2}$ the root mean squared (rms) charge radius calculated within HFB-17 and 0.88 fm the charge radius of the proton. CHFB-5DCH describes well the trend of the quadrupole collectivity beyond $A = 74$ but overpredicts the $B(E2)$ values towards the $N = Z$ line where shape coexistence

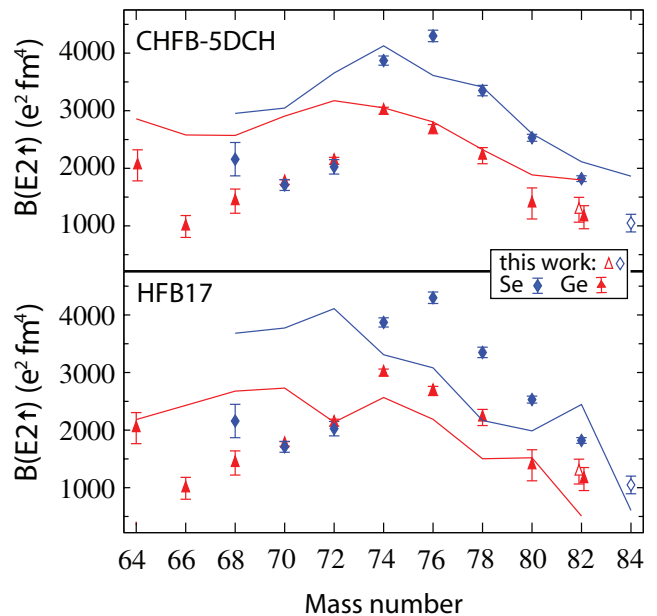


FIG. 5: (Color online) $B(E2; 0^+ \rightarrow 2_1^+)$ systematics of the selenium and germanium isotopic chains compared to calculations with the constrained Hartree-Fock Bogoliubov with mapping on the 5-dimensional collective Hamiltonian [37] approach (upper panel) and HFB calculations using the HFB-17 parameterization [38] (lower panel). Experimental values are taken from [6, 7, 13, 33, 35] and the present work.

dominates the nuclear structure. HFB-17 approximately reproduces the trend for the germanium isotopes heavier than $A = 70$ and at $N = Z$ but also overpredicts the collectivity for $A = 66 - 70$. The selenium isotopes are not well described by HFB-17.

B. Inelastic scattering from ^9Be

In addition to the Coulomb excitation, inelastic scattering off ^9Be was measured. Here, one expects nuclear excitations to dominate and to give access to states beyond the first 2^+ excitation in ^{84}Se and ^{82}Ge . A ^9Be target with a thickness of 188 mg/cm² was used to induce the inelastic excitations at 87.6 MeV/nucleon and 92 MeV/nucleon mid-target energies for ^{82}Ge and ^{84}Se , respectively.

The γ -ray spectra detected in coincidence with scattered ^{82}Ge and ^{84}Se are shown in Fig. 6. In the spectrum of ^{82}Ge , only the de-excitation of the first 2^+ state at 1348 keV is visible. Overlaid is the in-beam background obtained from an off-prompt gate on the trigger- γ -timing. The only obvious structures above background in ^{82}Ge are the full-energy peak of the $2_1^+ \rightarrow 0_1^+$ transition and its Compton edge. An excited state at 2287 keV in ^{82}Ge has been tentatively assigned as the 4_1^+ level from deep-inelastic reactions and spectroscopy of ^{248}Cm fission fragments [39, 40]. The corresponding γ -ray transition energy for the decay to the 2_1^+ level is $E_\gamma = 938$ keV. Un-

fortunately, the prompt background is very high at this energy and it was only possible to establish an upper limit of 60 counts in the full energy peak which corresponds to an upper limit for the cross section of $\sigma(4_1^+) \leq 4.8$ mb for ^{82}Ge . The cross sections for ^{82}Ge are given in Table III. The possible feeding from the decay of the 4^+ state is considered in the stated uncertainty of $\sigma(2_1^+)$. We note that the low statistics for ^{82}Ge might obscure the observation of additional weak feeding transitions.

In ^{84}Se , however, a second intense γ -ray transition at 667 keV is clearly visible in addition to the $2_1^+ \rightarrow 0_1^+$ decay. As shown in the inset, there is also evidence for two weaker γ -ray transitions at 2090 keV and 2462 keV. Excited states of ^{84}Se are known from $^{82}\text{Se}(t,p)^{84}\text{Se}$ two-neutron transfer reactions [41, 42], from γ -ray spectroscopy in $^{82}\text{Se}+^{192}\text{Os}$ deep-inelastic reactions [16], from prompt γ -ray detection following fission-fragment spectroscopy [43, 44] and from β decay [45, 46].

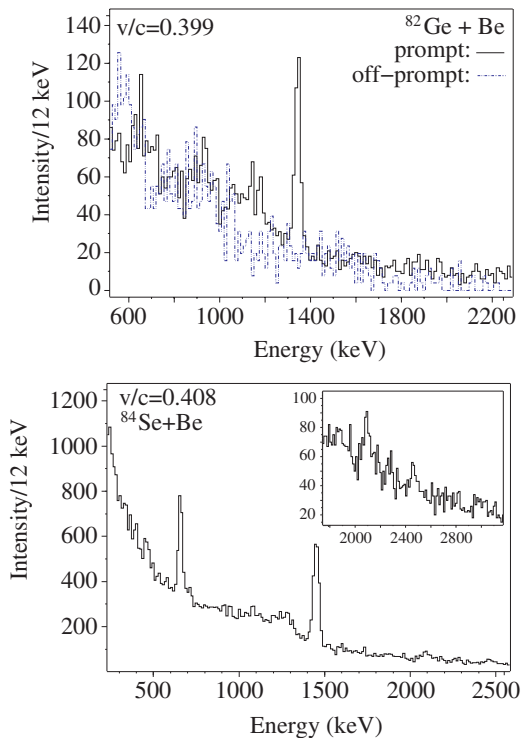


FIG. 6: (Color online) Event-by-event Doppler-reconstructed γ -ray spectra from $^{82}\text{Ge}+^9\text{Be}$ (upper panel) and $^{84}\text{Se}+^9\text{Be}$ (lower panel) inelastic scattering. The only γ -ray transition in ^{82}Ge is the $2_1^+ \rightarrow 0_1^+$ transition. An in-beam background spectrum, obtained from an off-prompt SeGA time gate, is overlaid. In the ^{84}Se spectrum, an intense γ -ray transition at 667(4) keV is observed in addition to the decay of the 2_1^+ state at 1454 keV.

The intense transition at 667 keV was reported in several of the previous measurements and has been attributed to the decay from the first 4^+ state to the 2^+ state, placing the 4_1^+ yrast level in ^{84}Se at 2122 keV excitation energy [16, 43, 44]. The transition at 2462 keV matches the energy of the ground-state decay of the sec-

ond 2^+ state. With the 2_2^+ state populated in the inelastic scattering, one would also expect to see its 1007 keV transition to the first 2^+ state at a branching ratio of 42% corresponding to about 80 counts. In the spectrum there seems to be no clear indication of a peak with this intensity, however, the background is high in this energy region. The 2090 keV transition could either be the ground-state decay of the (1^-) state at 2097(11) keV reported only from (t,p) two-neutron transfer [42], or – more likely – the 2087 keV transition that depopulates an excited state at 3542 keV with suggested $(2^+, 3^-)$ assignment based on the population in β decay [45, 46]. The second, weaker (15.8(7)% [47]) decay branch of this level to the 4^+ would not have been visible in our spectrum. The cross sections for ^{84}Se are summarized in Table III. The feeding from the decay of the 4^+ state was taken into account for the determination of the excitation cross section of the 2^+ state. The potential feeding by the 2090 keV transition and the decay of the 2_2^+ are included in the uncertainty.

TABLE III: Measured cross sections for $^{82}\text{Ge}+^9\text{Be}$ and $^{84}\text{Se}+^9\text{Be}$. The $\sigma(2^+)$ for ^{84}Se is corrected for the feeding by the 4_1^+ state. There is also evidence for weak higher-energy transitions at 2090(10) keV and 2462(11) keV. The placement of the 2090 keV line in the level scheme is unclear. The 2462 keV transition is likely the decay of the 2_2^+ to the ground state. The corresponding feeding by the $2_2^+ \rightarrow 2_1^+$ transition and the potential feeding by the 2090 keV transition has been taken into account in the error bars for $\sigma(2_1^+)$. The potential feeding of the 2_1^+ state of ^{82}Ge by the 4_1^+ decay has been folded into the uncertainty of the $\sigma(2_1^+)$ cross section.

σ (mb)	^{82}Ge	^{84}Se
$\sigma(2_1^+)$	27_{-6}^{+3}	20_{-6}^{+2}
$\sigma(4_1^+)$	≤ 4.8	12.4(12)
$\sigma(2090 \text{ keV})$	-	5(1)
$\sigma(2462 \text{ keV})$	-	2.9(7)

Inelastic α [48] and proton scattering [49–51] on the stable even-even selenium isotopes $^{74-82}\text{Se}$ revealed that the 2_1^+ states are excited the strongest, followed by the first 3^- and, at markedly less cross section, higher-lying 2^+ states and the 4_1^+ level. One might expect ^9Be -induced scattering to yield a similar population pattern, however, it seems for $^{84}\text{Se}+^9\text{Be}$ that the 4_1^+ state is more strongly excited than the 3^- state. Figure 7 shows the systematics of 3_1^- states in the selenium isotopes approaching ^{84}Se (upper panel) and in the $N = 50$ isotope chain heavier than selenium (lower panel). From both systematics one would expect the 3_1^- state in the $N = 50$ selenium nucleus to be around or above 3 MeV excitation energy. In fact, if ^{84}Se were to follow the trend established by the lighter isotopes, the state at 3542 keV would emerge as a good candidate. In the literature, 2^+ and $(2^+, 3^-)$ assignments based on β -decay measurements [45–47] can be found for this level. From the present work, both spin and parity assignments seem

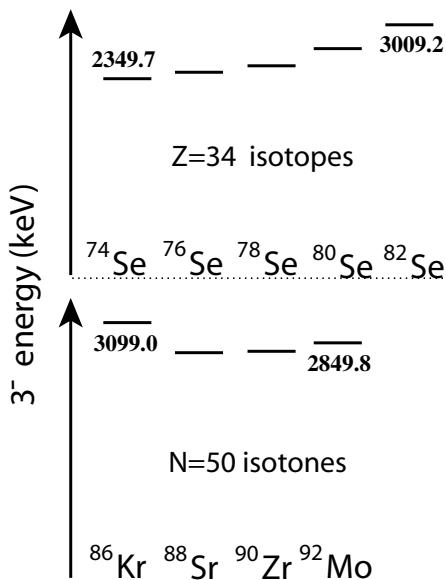


FIG. 7: Systematics of the 3_1^- states in the chain of Se isotopes (upper panel) and the $N = 50$ isotones (lower panel). From both systematics one would expect the first 3_1^- state in ^{84}Se to lie above or around 3 MeV excitation energy.

possible although if this level turns out to be a high-lying 2^+ state, the question emerges where the first 3_1^- state is located in ^{84}Se or why it is not as strongly excited in the inelastic scattering on ^9Be as one might expect from comparison with inelastic proton and α scattering on the stable selenium isotopes.

The role of the 4^+ state in ^{84}Se and its strong population in the ^9Be -induced inelastic scattering emerge as interesting. From inelastic scattering of polarized protons on $^{74-82}\text{Se}$, Matsuki *et al.* [49] present indications for a static or dynamic hexadecapole shape transition that occurs between the light ($^{74,76,78}\text{Se}$) and heavier ($^{80,82}\text{Se}$) selenium isotopes and point out that the hexadecapole degree of freedom plays an important role in the selenium isotopes. From inelastic proton scattering, Ogino *et al.* [50] find the hexadecapole strength fragmented strongly for $^{74-82}\text{Se}$. The transition strength to the 4_1^+ state was found to be rather weak except for the case of ^{82}Se where a transition strength of 1.3 spu was measured for the first 4^+ state [49, 50].

To help quantify these measured inelastic channel yields we have performed macroscopic (deformed) coupled-channels calculations [52]. The required projectile- ^9Be interactions were estimated by double-folding the point neutron and proton densities of ^{82}Ge and ^{84}Se (obtained from spherical Hartree-Fock calculations [53]) and of ^9Be (assumed a Gaussian with rms radius of 2.36 fm) with an effective nucleon-nucleon interaction [54]. Radii $R_0 = 1.1A^{1/3}$ fm were used in computing deformation lengths, $B(E2 \uparrow)$, etc. For ^{82}Ge , the $B(E2 \uparrow)$ of Table I is consistent with $\beta_2 = 0.2$, which gives a calculated $\sigma(2_1^+) = 21.9$ mb in line with that measured. Similarly for ^{84}Se , the $B(E2)$ of Ta-

ble I corresponds to $\beta_2 = 0.17$ ($\delta_2 = 0.83$ fm) giving $\sigma(2_1^+) = 15.2$ mb and, in the absence of hexadecapole deformation $\sigma(4_1^+) = 0.05$ mb. When including $|\beta_4| = 0.05$ (1.3 spu) as was deduced for the $^{82}\text{Se}(4_1^+)$ state [49], $\sigma(4_1^+) = 1.12$ mb and with $|\beta_4| = 0.08$ (3 spu), being the maximum hexadecapole strength observed in the neighboring selenium isotopes [50], we obtain $\sigma(4_1^+) = 2.25$ mb. This remains considerably adrift from the observed $^{84}\text{Se}(4_1^+)$ yield. To reproduce the measured cross sections of Table III, using the coupled-channels model calculations described here, would require the use of $\beta_2 = \beta_4 \approx 0.2$, giving $\sigma(2_1^+) = 18.5$ mb and $\sigma(4_1^+) = 12.0$ mb.

IV. SUMMARY

In summary, the $B(E2; 0_1^+ \rightarrow 2_1^+)$ excitation strengths were measured for ^{82}Ge and ^{84}Se using intermediate-energy Coulomb excitation. The quadrupole collectivity along the $N = 50$ isotone chain from zinc to molybdenum is compared to large-scale shell-model calculations with three different effective interactions. The calculated $B(E2)$ values for ^{82}Ge and ^{84}Se were found sensitive to the size of the ESPE gap between the $p_{3/2}$ and $f_{5/2}$ orbits in ^{78}Ni and ^{88}Sr . From comparison to experiment it is indicated that the relevant ESPE gap for the jj4pna effective interaction is too small at $Z = 34$ while the JUN45 Hamiltonian predicts the $E2$ strength fragmented over the first and second 2^+ states.

The quadrupole collectivity along the germanium and selenium chains is compared to Skyrme Hartree-Fock Bogoliubov (HFB) calculations using the HFB-17 force and to constrained HFB calculations extended by the generator coordinate method and mapped onto a 5-dimensional collective quadrupole Hamiltonian (CHFB-5DCH with Gogny D1S force). CHFB-5DCH describes well the trend of the quadrupole collectivity beyond $A = 74$ for both isotopic chains but overpredicts the $B(E2 \uparrow)$ values towards the $N = Z$ line where shape-coexistence occurs. HFB-17 approximately reproduces the trend for the germanium isotopes heavier than $A = 70$ and at $N = Z$ but also overestimates the collectivity between $A = 66$ and 70. The selenium isotopes are not well described by the HFB-17 parameterization.

In ^9Be -induced inelastic scattering, the first 4^+ state of ^{84}Se was populated with significant intensity while there was no indication of a similarly strong population of the corresponding state in ^{82}Ge . The excitation of the 4^+ state is discussed in comparison to inelastic α and proton scattering data on stable selenium nuclei and coupled-channels calculations, however, its explanation remains a challenge for future reaction theory and nuclear structure calculations.

Acknowledgments

A.G. acknowledges discussions with Kirby W. Kemper (FSU), Paul D. Cottle (FSU) and Lewis A. Riley (Ursinus). This work was supported by the National Science

Foundation under Grants No. PHY-0606007 and PHY-0758099 and the UK Science and Technology Facilities Council (Grant ST/F012012). A.G. is supported by the Alfred P. Sloan Foundation.

-
- [1] M. Sugawara *et al.*, *Eur. Phys. J. A* **16**, 409 (2003).
 [2] B. Kotlinski *et al.*, *Nucl. Phys.* **A519**, 646 (1990).
 [3] Y. Toh *et al.*, *Eur. Phys. J. A* **9**, 353 (2000).
 [4] Y. Toh *et al.*, *J. Phys. G* **27**, 1475 (2001).
 [5] H. T. Fortune and M. Carchidi, *Phys. Rev. C* **36**, 2584 (1987).
 [6] K. Starosta *et al.*, *Phys. Rev. Lett.* **99**, 042503 (2007).
 [7] A. Obertelli *et al.*, *Phys. Rev. C* **80**, 031304(R) (2009).
 [8] J. H. Hamilton, A. V. Ramayya, W. T. Pinkston, R. M. Ronningen, G. Garcia-Bermudez, and H. K. Carter, R. L. Robinson, H. J. Kim, and R. O. Sayer, *Phys. Rev. Lett.* **32**, 239 (1974).
 [9] J. H. Hamilton *et al.*, *Phys. Rev. Lett.* **36**, 340 (1976).
 [10] J. Heese, K. P. Lieb, L. Lühmann, F. Raether, B. Wörmann, D. Alber, H. Grawe, J. Eberth, and T. Mylaeus, *Z. Phys. A* **325**, 45 (1986).
 [11] S. M. Fischer *et al.*, *Phys. Rev. Lett.* **84**, 4064 (2000).
 [12] A. M. Hurst *et al.*, *Phys. Rev. Lett.* **98**, 072501 (2007).
 [13] J. Ljungvall *et al.*, *Phys. Rev. Lett.* **100**, 102502 (2008).
 [14] D. Verney *et al.*, *Phys. Rev. C* **76**, 054312 (2007).
 [15] M. Lebois *et al.*, *Phys. Rev. C* **80**, 044308 (2009).
 [16] Y. H. Zhang *et al.*, *Phys. Rev. C* **70**, 024301 (2004).
 [17] J. Van der Walle *et al.*, *Phys. Rev. Lett.* **99**, 142501 (2007).
 [18] J. Hakala *et al.*, *Phys. Rev. Lett.* **101**, 052502 (2008).
 [19] A. F. Lisetskiy *et al.*, *Phys. Rev. C* **70**, 044314 (2004).
 [20] M. Honma, T. Otsuka, T. Mizusaki, and M. Hjorth-Jensen, *Phys. Rev. C* **80**, 064323 (2009).
 [21] D. J. Morrissey *et al.*, *Nucl. Instrum. Methods in Phys. Res., Sect. B* **204**, 90 (2003).
 [22] D. Bazin *et al.*, *Nucl. Instrum. Methods in Phys. Res., Sect. B* **204**, 629 (2003).
 [23] J. Yurkon, D. Bazin, W. Benenson, D. J. Morrissey, B. M. Sherrill, D. Swan, and R. Swanson, *Nucl. Instrum. Methods in Phys. Res., Sect. A* **422**, 291 (1999).
 [24] W. F. Mueller *et al.*, *Nucl. Instr. and Methods in Phys. Res., Sect. A* **466**, 492 (2001).
 [25] T. Glasmacher, *Annu. Rev. Nucl. Part. Sci.* **48**, 1 (1998).
 [26] T. Motobayashi, Y. Ikeda, K. Ieki, M. Inoue, N. Iwasa, T. Kikuchi, M. Kurokawa, S. Moriya, S. Ogawa, H. Murakami, S. Shimoura, Y. Yanagisawa, T. Nakamura, Y. Watanabe, M. Ishihara, T. Teranishi, H. Okuno and R. F. Casten, *Phys. Lett. B* **346**, 9 (1995).
 [27] S. Wan *et al.*, *Eur. Phys. J. A* **6**, 167 (1999).
 [28] A. Gade and T. Glasmacher, *Prog. Part. Nucl. Phys.* **60**, 161 (2008).
 [29] F. Delaunay and F. M. Nunes, *J. Phys. G* **34**, 2207 (2007).
 [30] J. M. Cook, T. Glasmacher, A. Gade, *Phys. Rev. C* **73**, 024315 (2006).
 [31] A. Winther and K. Alder, *Nucl. Phys.* **A319**, 518 (1979).
 [32] C. Zhou, *Nucl. Data Sheets* **76**, 399 (1995).
 [33] E. Padilla-Rodal *et al.*, *Phys. Rev. Lett.* **94**, 122501 (2005).
 [34] X. Ji and B. H. Wildenthal, *Phys. Rev. C* **38**, 2849 (1988).
 [35] S. Raman, C. W. Nestor, and P. Tikkanen, *At. Data and Nuclear Data Tables* **78**, 1 (2001).
 [36] C. M. Baglin, *Nuclear Data Sheets* **91**, 423 (2000).
 [37] J. P. Delaroche, M. Girod, J. Libert, H. Goutte, S. Hilaire, S. Peru, N. Pillet, G. F. Bertsch, *Phys. Rev. C* **81**, 014303 (2010).
 [38] S. Goriely, N. Chamel, and J. M. Pearson, *Phys. Rev. Lett.* **102**, 152503 (2009).
 [39] G. de Angelis, *Nucl. Phys.* **A787**, 74 (2007).
 [40] T. Rzaca-Urban *et al.*, *Phys. Rev. C* **76**, 027302 (2007).
 [41] J. D. Knight, C. J. Orth, W. T. Leland, and A. B. Tucker, *Phys. Rev. C* **9**, 1467 (1974).
 [42] S. M. Mullins *et al.*, *Phys. Rev. C* **37**, 587 (1988).
 [43] A. Prevost *et al.*, *Eur. Phys. J. A* **22**, 391 (2004).
 [44] E. F. Jones *et al.*, *Phys. Rev. C* **73**, 017301 (2006).
 [45] J. V. Kratz, H. Franz, N. Kaffrel, and G. Herrmann, *Nucl. Phys.* **A250**, 13 (1975).
 [46] P. Hoff, B. Ekström, B. Fogelberg, J.P. Omtvedt, *Z. Phys. A* **338**, 285 (1991).
 [47] National Nuclear Data Center (<http://www.nndc.bnl.gov/>).
 [48] F. Ballester, E. Casal, J. B. A. England, and F. Moriano, *J. Phys. G* **14**, 1103 (1988).
 [49] S. Matsuki *et al.*, *Phys. Rev. Lett.* **51**, 1741 (1983).
 [50] K. Ogino, *Phys. Rev. C* **33**, 71 (1989).
 [51] J. P. Delaroche, R. L. Varner, T. B. Clegg, R. E. Anderson, B. L. Burks, E. J. Ludwig, and J. F. Wilkerson, *Nucl. Phys.* **A414**, 113 (1984).
 [52] I.J. Thompson, Computer code FRESKO. Available at <http://www.fresco.org.uk/index.htm>. See also, I.J. Thompson, *Comp. Phys. Rep.*, **7**, 167 (1988).
 [53] B. A. Brown, *Phys. Rev. C* **58**, 220 (1998).
 [54] J.A. Tostevin, G. Podolyák, B.A. Brown and P.G. Hansen, *Phys. Rev. C* **70**, 064602 (2004).
 [55] We note that the neutron effective charge is irrelevant since a closed neutron shell is assumed in the shell model and thus $A_n = 0$ in $B(E2 \uparrow) = (A_p e_p + A_n e_n)^2$